Functional Architecture of the Inner Pore of a Voltage-gated Ca^{2+} Channel

Xiao-guang Zhen, Cheng Xie, Aileen Fitzmaurice, Carl E. Schoonover, Eleza T. Orenstein, and Jian Yang

Department of Biological Sciences, Columbia University, New York, NY 10027

The inner pore of voltage-gated Ca^{2+} channels (VGCCs) is functionally important, but little is known about the architecture of this region. In K$^+$ channels, this part of the pore is formed by the S6/M2 transmembrane segments from four symmetrically arranged subunits. The Ca^{2+} channel pore, however, is formed by four asymmetric domains of the same (α_1) subunit. Here we investigated the architecture of the inner pore of P/Q-type Ca^{2+} channels using the substituted-cysteine accessibility method. Many positions in the S6 segments of all four repeats of the α_1 subunit (Ca$_v$2.1) were modified by internal methanethiosulfonate ethyltrimethylammonium (MTSET). However, the pattern of modification does not fit any known sequence alignment with K$^+$ channels. In IIS6, five consecutive positions showed clear modification, suggesting a likely aqueous crevice and a loose packing between S6 and S5 segments, a notion further supported by the observation that some S5 positions were also accessible to internal MTSET. These results indicate that the inner pore of VGCCs is indeed formed by the S6 segments but is different from that of K$^+$ channels. Interestingly some residues in IIIS6 and IVS6 whose mutations in L-type Ca^{2+} channels affect the binding of dihydropyridines and phenylalkylamines and are thought to face the pore appeared not to react with internal MTSET. Probing with qBBr, a rigid thiol-reactive agent with a dimension of 12 Å $\times$ 10 Å $\times$ 6 Å suggests that the inner pore can open to >10 Å. This work provides an impetus for future studies on ion permeation, gating, and drug binding of VGCCs.

INTRODUCTION

Among the extended family of voltage-gated ion channels, VGCCs (voltage-gated Ca^{2+} channels) are of particular functional importance. Opening of these channels not only changes the membrane potential, but the resulting influx of Ca^{2+} ions also serves as a second messenger, initiating diverse events such as contraction, secretion, synaptic transmission, and gene expression. Physiological and pharmacological studies have identified multiple types of voltage-gated calcium currents, including L, N, P/Q, R, and T. Biochemical and molecular studies show that VGCCs are multimeric complexes of several distinct subunits: α_1, β, $\alpha_2\delta$, and sometimes γ. The different types of Ca^{2+} currents are defined by different α_1 subunits (Catterall, 2000). As the primary subunit, α_1 is equipped with most functions of the channel: it forms the ion conduction pore, incorporates the voltage sensor and gating apparatus, and carries many sites for regulation by second messengers, G proteins, protein kinases and phosphatases, agonists, antagonists, and toxins. The topology of various α_1 subunits is the same, containing four homologous repeats, each consisting of six transmembrane segments (S1–S6) and a pore loop (P-loop) between S5 and S6 (Fig. 1 A). The β and $\alpha_2\delta$ subunits are auxiliary subunits and regulate channel assembly, trafficking, membrane

targeting, activation, and inactivation properties (Catterall, 2000).

Previous structure–function studies on VGCCs show that the P-loop, which harbors four conserved glutamate residues, forms the ion selectivity filter and is critical for Ca^{2+} selectivity and permeation (Kim et al., 1993; Tang et al., 1993; Yang et al., 1993; Ellinor et al., 1995). The inner pore of VGCCs is also likely to be important for Ca^{2+} permeation as well as for gating, as in K$^+$ channels. It also harbors binding sites for organic molecules such as phenylalkylamines (PAAs), benzothiazepines (BTZs), and dihydropyridines (DHPs) (Peterson et al., 1996, 1997; Hockerman et al., 1995, 1997a,b), which are commonly used drugs for the treatment of cardiovascular diseases. In K$^+$ channels, the inner pore is formed by the S6/M2 transmembrane segments from four symmetrically arranged subunits, as revealed by site-directed chemical modifications and x-ray crystallography (Liu et al., 1997; Doyle et al., 1998; Lu et al., 1999a; Jiang et al., 2002a,b, 2003a,b). By contrast, little is known about the architecture of the inner pore of VGCCs, which are thought to be evolved from K$^+$ channels but their pore is formed by four

X.-g. Zhen and C. Xie contributed equally to this work.

Correspondence to Jian Yang: jy160@columbia.edu

Abbreviations used in this paper: BTZ, benzothiazepine; DHP, dihydropyridine; MTSET, methanethiosulfonate ethyltrimethylammonium; PAA, phenylalkylamine; SCAM, substituted-cysteine accessibility method; VGCC, voltage-gated Ca^{2+} channel.

asymmetric domains of the same (α_1) subunit. There is yet no systematic analysis of which transmembrane regions and amino acids form the inner pore of VGCCs.

In this study, we investigated the architecture of the inner pore of P/Q-type (Ca$_v$2.1) Ca^{2+} channels using the substituted-cysteine accessibility method (SCAM), which has been used in various types of channels to identify pore-lining residues, size the channel, examine the conformational changes in different functional states, and locate the activation gate (e.g., Akabas et al., 1992, 1994; Yang and Horn, 1995; Liu et al., 1997; Lu et al., 1999a,b; Liu and Siegelbaum, 2000; Wu et al., 2000; del Camino and Yellen, 2001; Flynn and Zagotta, 2001; Xiao et al., 2003; for review see Karlin and Akabas, 1998). We systematically mutated residues of all four S6 segments of the α_1 subunit (Ca$_v$2.1) to cysteines, one at a time, and probed the mutant channel with a water-soluble sulfhydryl-specific reagent, which forms a covalent bond with the sulfhydryl group on the accessible cysteine. Our results indicate that the inner pore of VGCCs shares some properties with that of K$^+$ channels but also possesses certain unique and surprising features. Thus, many positions in the S6 segments of all four repeats were found to be modified by internal methanethiosulfonate ethyltrimethylammonium (MT-SET), indicating that the inner pore of VGCCs is indeed formed by S6. However, the pattern of modification does not fit any known sequence alignment with K$^+$ channels and is consistent with an asymmetric architecture. In IIS6, five consecutive positions showed clear modification, suggesting a likely aqueous crevice between S6 and S5 segments, a notion further supported by the observation that some S5 positions were also accessible to internal MTSET. This loose packing of the S6 and S5 segments is different from the tight packing in K$^+$ channels. Finally, some residues in IIIS6 and IVS6 whose mutations in L-type (Ca$_v$1.2) channels affect the binding of DHPs and/or PAAs and are thought to face the pore appeared not to react with internal MTSET.

MATERIALS AND METHODS

Molecular Biology

Ca$_v$2.1 (GenBank/EMBL/DDBJ accession no. X57689) and $\alpha_2\delta$ (Mikami et al., 1989) cDNAs are from rabbit brain and skeletal muscle, respectively. β_{2a} cDNA (M80545) is from rat brain. Site-directed mutations were generated by either PCR mutagenesis or the oligo nucleotide insertion method and were confirmed by sequencing. Eight endogenous cysteines in the N terminus, intracellular loops, IVS6, and C terminus of Ca$_v$2.1 were mutated to alanines. The channel formed by this mutant subunit and the $\alpha_2\delta$ and β subunits is called "the control channel." All cysteine mutations were made on this "control" α_1 subunit. All α_1 constructs and $\alpha_2\delta$ were cloned in an oocyte expression vector, pGEMHE, or one of its variants. The β_{2a} subunit was cloned in the Bluescript SK vector; it was chosen because it confers the slowest inactivation, which greatly facilitates our experiments. cRNA for all constructs were transcribed in vitro using the T7 polymerase.

Oocyte Expression

Ovarian lobes were obtained from adult *Xenopus laevis* under anesthesia. Stage V–VI oocytes were prepared by treatment with 2 mg/ml collagenase A (Roche) for 1.5–2.5 h under 200 rpm shaking in a solution containing 82.4 mM NaCl, 2.5 mM KCl, 1 mM MgCl$_2$, and 5 mM HEPES (pH 7.6) and then rinsed twice (15 min each) with ND96 solution containing 96 mM NaCl, 2.5 mM KCl, 1 mM MgCl$_2$, 5 mM HEPES, 1.8 mM CaCl$_2$, 100 U/ml penicillin, and 100 μg/ml streptomycin (pH 7.6). The α_1, $\alpha_2\delta$, and β_{2a} cRNA were injected into defoliculated oocytes with a total concentration of $\sim$0.5 μg/μl (ratio α_1:$\alpha_2\delta$:β_{2a} = 5:5:4) and a volume of $\sim$50 nl per oocyte. Injected oocytes were maintained in ND96 solution in an 18°C incubator, and used for recordings 3–6 d after injection.

Electrophysiology

Whole-cell currents recorded with two-electrode voltage-clamp with the OC-725C oocyte clamp amplifier (Warner Instruments) were used mainly for checking the functional expression of mutant channels in oocytes. The recording electrodes were filled with 3 M KCl and had resistances of $\sim$0.5–1 MΩ. The bath solution contained 10 mM BaCl$_2$, 5 mM KCl, 60 mM TEA-OH, 20 mM NaOH, and 5 mM HEPES (pH 7.4 with methanesulfonic acid).

All patch-clamp recordings were performed using the inside-out configuration. Oocyte was bathed in a bath solution containing 125 mM KCl, 4 mM NaCl, 10 mM HEPES, 10 mM EGTA (pH 7.3 with KOH). The control solution, which in addition contained 2 mM Mg-ATP and 3 μM sonicated PIP$_2$, was prepared fresh daily. Recording glass pipettes pulled from pyrex glass tubes (Corning) were filled with a solution of 85 mM BaCl$_2$, 10 mM HEPES (pH 7.3 with KOH), and had a resistance of 0.2–0.3 MΩ. When monovalent current was recorded, the pipettes were filled with the bath solution. Control and test solutions (with the reagent dissolved in the control solution) were fed by gravity through separate tubes to a manifold attached to a single outlet tube and were switched on/off individually. After obtaining the inside-out patches, the recording pipette was inserted into the perfusion tube to achieve a rapid and complete exchange of solution.

Patch-clamp recordings were performed with the Axopatch 200A amplifier (Axon Instruments). Macroscopic currents were evoked from a holding potential of -80 mV every 6 s by a 500-ms depolarization to a voltage that opens >70% of the channels (0 to 40 mV, depending on the channel type). To examine the voltage dependence of activation, currents were evoked from a holding potential of -80 mV every 3 s by 10-ms test potentials from -30 to $+100$ mV in 10-mV increments, followed by a 50-ms repolarization to -30 mV. Activation curves were constructed by plotting the tail currents at -30 mV against the test potentials. Reversal potential was interpolated from current–voltage curves. All currents were filtered at 2 kHz, digitized at 10 kHz. Data acquisition and analysis were performed using pClamp8 (Axon Instruments) on a PC through a Digidata 1200 interface. Experiments were performed at 21–23°C.

MTS reagents (Toronto Research Chemicals) and qBBr (Molecular Probes) were stored at -20°C and were dissolved in the control solution before each experiment, generally <5 min before application. 4 mM MTS reagents and qBBr were applied for 2–8 min, until modification reached a steady state or the speed of modification could not be distinguished from that of intrinsic current rundown. The effect of a reagent was calculated from the current amplitude obtained before application and after washout of the reagents. Data are represented as mean $\pm$ SD (number of observations). Significance was determined using the Mann-Whitney Test. No corrections were made for leakage current, which was negligible at -80 to 100 mV in macropatch recordings.
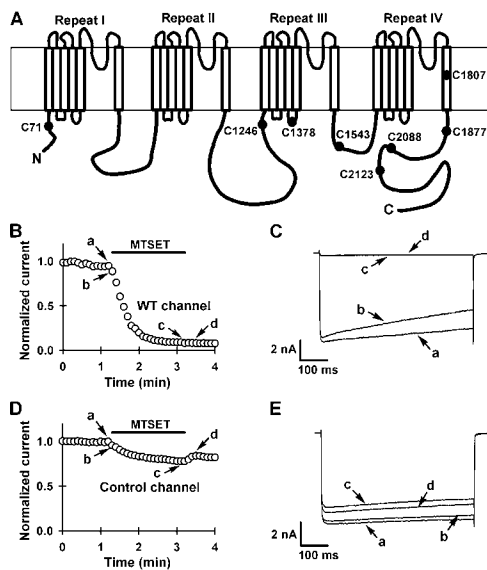
Figure 1. Construction of a control channel nonreactive to internal MTSET. (A) Putative transmembrane topology of the $\alpha 1$ subunit of a voltage-gated Ca^{2+} channel. Black dots show the location of the endogenous cysteines that were substituted with alanines. (B and D) Time course of inhibition of the wild-type channel (B) and control channel (D) by 4 mM internal MTSET. Current was evoked from a holding potential of -80 mV every 6 s by a 500-ms depolarization to $+30$ mV. (C and E) Exemplar current traces of the wild-type channel (C) and control channel (E) taken immediately before (a) and after (b) MTSET application and immediately before (c) and after (d) washout of MTSET, as indicated in B and D.

RESULTS

Controlling Rundown of P/Q-type Channels

The activity of P/Q-type channels is stable in cell-attached patches, but decreases rapidly and disappears eventually when a membrane patch is excised into the inside-out configuration. The speed of this rundown is relatively constant among the same batch of oocytes but varies from batch to batch. To examine cysteine modification by an internal reagent, we first needed to prevent or slow down channel rundown. Our previous work indicates that this can be accomplished by perfusing the membrane with a bath solution containing Mg-ATP (2 mM) and a low concentration (3 μM) of PIP_2 immediately after patch excision (Wu et al., 2002). With such a treatment, the remaining current obtained 10 min after patch excision increased from 34.1% (normalized by the current measured immediately after patch excision) in the bath solution to 85.6% ($n = 6$). This reduced rundown permitted us to carry out the cysteine modification experiments.

Construction of a Control Channel Nonreactive to Sulfhydryl-specific Modifying Reagents

Another prerequisite for using SCAM is the ability to clearly distinguish the response of the cysteine mu-
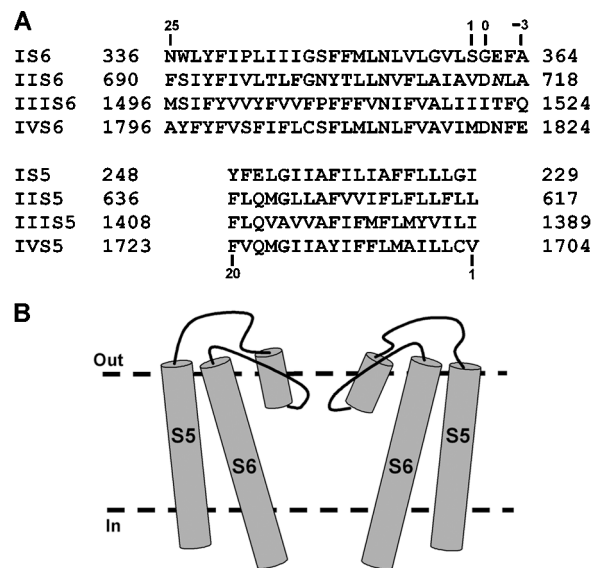

Figure 2. Amino acid sequences and schematic topology. (A) Amino acid sequence of S6 and S5 segments in the four repeats of the $Ca_v2.1$ subunit. Amino acid numbers are given on both sides. The numeration of residues in each repeat defined in this study is shown on the top and bottom. Position 0 presumably represents the membrane/cytoplasm interface. (B). Schematic topology of the S5 and S6 segments and the P-loop of two repeats.

tant channels from that of the wild-type channel. The $Ca_v2.1$ subunit used in our experiments contains 28 endogenous cysteines, out of which nine are in the extracellular and intracellular loops, respectively, nine in the transmembrane segments, and one in the P-loop. Despite the presence of nine extracellular cysteines, external MTS reagents did not produce significant irreversible current inhibition in the wild-type channel (unpublished data). Similar lack of effect by extracellular sulfhydryl modifiers was also observed in the cardiac L-type Ca^{2+} channel (Wu et al., 2000). On the other hand, the wild-type P/Q-type channel was irreversibly and completely inhibited by internal MTSEA or MTSET (Fig. 1, B and C), indicating that one or more endogenous cysteines were covalently modified. To eliminate the intrinsic reactivity with internal modifiers, we substituted alanine for eight endogenous cysteines in the NH_2 terminus (C71), intracellular loops (C1246, C1378, and C1543), COOH terminus (C1877, C2088, and C2123), and IVS6 (C1807) in the α_1 subunit (Fig. 1 A). The channel formed by this mutant α_1 subunit with $\alpha_2\delta$ and β subunits was called "the control channel." It was functional and generated large macroscopic currents in oocytes, the amplitude of which was comparable to that produced by wild-type channels. The activation voltage of the control channel was shifted by -20 mV but the speed of inactivation was little affected (Table I). Importantly, the control channel did not show significant reactivity with internal MTSEA or MTSET

TABLE I

Summary of the Effect of MTSET on IS6 Cysteine Mutant Channels

	Positions in IS6	MTSET inhibition	Reversal potential	Activation $V_{1/2}$	Slope factor k	τ at 0 mV	Inactivation before modification	Inactivation after modification
		%	mV	mV	mV	ms	%	%
WT		100.0 ± 0.0 (6)	84.4 ± 2.8	26.0 ± 2.6	8.6 ± 1.3	4.4 ± 2.0[a]	9.5 ± 3.9	
Control		19.0 ± 5.9 (20)	82.7 ± 4.8	6.6 ± 3.6	9.0 ± 0.9	5.4 ± 2.2	8.1 ± 4.2	14.5 ± 4.4
G347C	14	23.2 ± 7.6 (6)	73.2 ± 13.0	3.4 ± 6.9	10.6 ± 1.1	3.2 ± 1.0	14.2 ± 5.6	19.9 ± 19.3
S348C	13	45.1 ± 11.0 (4)	81.1 ± 6.9	1.5 ± 5.8	8.1 ± 1.0	6.7 ± 1.1	32.3 ± 13.5	46.1 ± 15.2
F349C	12	37.5 ± 9.5 (4)	83.3 ± 4.8	12.3 ± 8.3	12.2 ± 2.6	8.2 ± 8.8	30.1 ± 15.4	41.9 ± 19.1
F350C	11	25.6 ± 10.5 (6)	74.8 ± 8.8	−0.3 ± 6.1	10.7 ± 1.7	4.0 ± 1.8	14.1 ± 9.5	27.1 ± 21.9
M351C	10	15.3 ± 6.4 (3)	84.0 ± 5.0	6.1 ± 2.9	9.6 ± 0.6	8.0 ± 2.3	8.5 ± 7.8	15.5 ± 15.3
L352C	9	57.2 ± 8.3 (5)	82.2 ± 3.3	16.8 ± 7.1	13.6 ± 0.9	3.4 ± 0.9	50.3 ± 8.3	60.6 ± 5.0
L354C	7	28.2 ± 8.1 (3)	72.7 ± 10.1	33.5 ± 2.5	21.7 ± 2.6	1.6 ± 0.6	28.1 ± 13.3	40.1 ± 28.3
V355C	6	18.1 ± 10.4 (4)	78.3 ± 10.7	5.6 ± 9.4	8.3 ± 1.6	8.4 ± 6.3	19.5 ± 17.0	26.5 ± 20.2
L356C	5	81.2 ± 4.0 (4)	71.5 ± 10.3	1.4 ± 5.8	9.4 ± 1.1	5.9 ± 1.8	5.1 ± 3.8	7.7 ± 2.7
G357C	4	86.8 ± 3.7 (3)	68.5 ± 2.1	87.6 ± 1.7	15.1 ± 1.5	1.7 ± 0.2	51.1 ± 5.5	22.0 ± 4.6
V358C	3	15.3 ± 3.7 (7)	74.1 ± 6.6	−2.1 ± 10.8	8.7 ± 3.2	4.0 ± 1.4	10.1 ± 16.6	14.7 ± 19.6
L359C	2	67.7 ± 2.9 (4)	76.8 ± 3.0	−5.9 ± 3.9	8.8 ± 1.4	5.2 ± 2.8	16.7 ± 7.3	36.3 ± 6.3
S360C	1	86.4 ± 7.4 (5)	84.4 ± 1.7	28.5 ± 3.3	15.6 ± 0.7	3.5 ± 1.1	41.3 ± 20.7	76.2 ± 8.8
G361C	0	46.9 ± 4.0 (5)	68.4 ± 3.8	−3.9 ± 4.7	8.7 ± 2.1	2.8 ± 1.6	16.8 ± 6.4	10.5 ± 3.4
E362C	−1	9.2 ± 6.5 (5)	82.4 ± 4.5	19.9 ± 1.7	12.5 ± 0.6	3.0 ± 1.2	25.6 ± 7.7	40.8 ± 3.7
F363C	−2	98.8 ± 1.2 (5)	77.8 ± 6.5	−10.8 ± 7.2	10.4 ± 3.3	3.1 ± 2.7	37.7 ± 15.5	
A364C	−3	40.2 ± 5.6 (8)	77.5 ± 5.8	−3.8 ± 3.6	8.7 ± 0.8	3.8 ± 1.4	13.2 ± 4.4	35.9 ± 6.6

Summary of the effect of MTSET on the S6 cysteine mutant channels in all four repeats. Also included are some of the activation and inactivation properties of the mutant channels. The data for the reversal potential, half-activation voltage ($V_{1/2}$), slope factor (k) and time constant (τ) of activation at 0 mV were obtained from the cell-attached configuration. Inactivation was calculated as the ratio of the current decrease and the peak current during the 500-ms depolarization. Inactivation was not determined for some mutant channels due to the small residual current after MTSET modification.

[a]Time constant of activation at +20 mV was calculated for the wild-type channel because open probability of the channel is very low at 0 mV.

(Fig. 1, D and E), and it was also nonreactive to external MTS reagents (not depicted). Furthermore, the activity of the control channel could still be stabilized by Mg-ATP (2 mM) + PIP$_2$ (3 μM) in inside-out patches.

S6 Transmembrane Segments Form the Inner Pore

After overcoming the two technical obstacles for using SCAM, we began to identify residues that may form the inner pore, focusing on the S6 segments of the α_1 subunit. We aligned the amino acid sequence of all four S6 segments based on a conserved asparagine (Fig. 2 A, top). The putative residue at the interface of the membrane and cytoplasm is defined as position 0. Residues in the membrane are numbered as 1, 2, 3, etc., from inside to outside, and residues beyond the membrane are numbered as −1, −2, −3, etc. To determine putative pore-lining residues, we replaced, one by one, a total of 87 consecutive residues in all four S6 segments with a cysteine, mainly from position 14 to position −3 in each repeat. All but five mutant α_1 subunits formed functional channels in oocyte. The five mutants that failed to produce large enough Ba^{2+} currents are IS6-N8C, IIIS6-Y18C, IIIS6-V20C, IVS6-L7C and IVS6-N8C.

The effect of internal MTSET on currents mediated by the S6 cysteine mutant channels is summarized in

Fig. 3. Some mutant channels did not show significant functional change after exposure to MTSET (as exemplified in Fig. 4 A), suggesting that these residues do not line the pore. Many mutant channels, however, showed varying degrees of irreversible inhibition (as exemplified in Fig. 4, B and C). The side chain of these residues is presumably exposed to the aqueous pore. Among the eight IIIS6 NH$_2$ terminus residues (from IIIS6-15 to IIIS6-25 except for two nonfunctional channels and one mutant whose DNA was not constructed due to some technical problems), only one (IIIS6-F22C) was partially modified by MTSET, suggesting that this part of the S6 might be buried behind the selectivity filter and pore helix, as it is in K$^+$ channels. When the results are represented in an α-helical wheel (Fig. 5), most of the MTSET-reactive positions are located on one side of the S6 helices, supporting the interpretation that they face the lumen of the pore. These results indicate that the S6 segments form the Ca^{2+} channel inner pore. Notice, however, that the reactive side is broader than the nonreactive side and some reactive positions are located on the back side of the helical wheel. These results will be discussed later.

Many of the residues that are presumably at or below the membrane boundary (position 0 to position −3 in
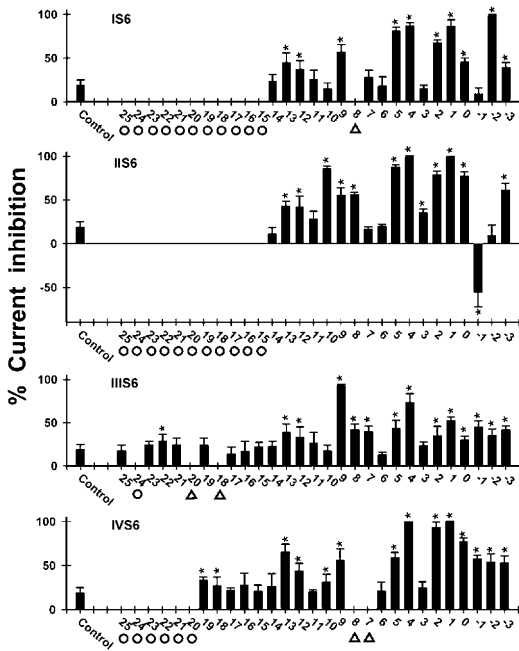
Figure 3. Summary of the effect of MTSET on S6 mutant channels. Bars represent current inhibition by 4 mM internal MTSET on the control channel ($n = 20$) and S6 cysteine mutant channels ($n = 3–15$). Stars indicate mutant channels that were significantly inhibited compared with the control channel ($P < 0.05$). Circles and triangles indicate, respectively, positions that were either not mutated or mutated but failed to produce functional channels. Original data are summarized in Tables I–IV. Experiment conditions were the same as in Fig. 4 A.

Figure 5. Helical wheel representation of MTSET modification of S6 positions. The effect of internal MTSET on the cysteine mutant channels (position 1–14) for each S6 segment is shown in an α-helix wheel. Filled circles indicate positions that were modified by MTSET and open circles indicate those that were not modified. Cysteine mutant channels that had no function are shown in little black dots.

each repeat), also showed different degrees of modification, and modification of one position, IIS6-N-1C, showed a current increase of $55.6 \pm 16.5\%$ ($n = 7$) (Fig. 3). Since MTSET could reach these positions from all directions around the presumed helices, modification of these residues does not necessarily mean that they face the ion conduction pathway. It is possible that the effect of MTSET on at least some of these mutant channels, especially the augmentation of IIS6-N-1C, is an allosteric effect.

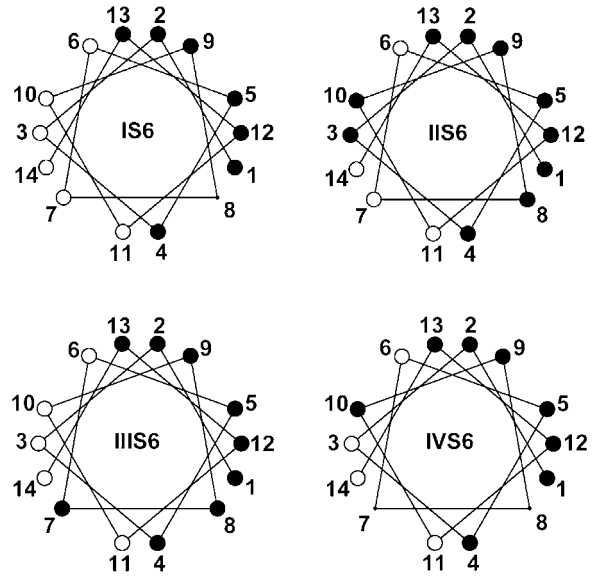To determine whether the functional effect of MTSET on the S6 mutants is due to a change of gating, we examined the voltage dependence of activation before and after MTSET application for four mutant channels, one in each repeat (IS6-L2C, IIS6-N-1C, IIIS6-A4C, and IVS6-V5C). The activation curves of these channels were not significantly altered after modification, as exemplified in Fig. 6. Thus, covalent modification by MTSET most likely inhibits these mutant channels by blocking the ion conduction pathway rather than by changing channel gating. However, MTSET may inhibit currents by different mechanisms at different positions, either by blocking ion conduction or changing gating, or both.

Some Positions in the S5 Segments Are Accessible

As mentioned above, the MTSET-reactive surface of all four S6 segments is broad (Fig. 5). In IIS6, five consecutive positions showed clear modification (Fig. 3). Furthermore, some reactive positions are located on the back side of the helical wheel (Fig. 5). This pattern of
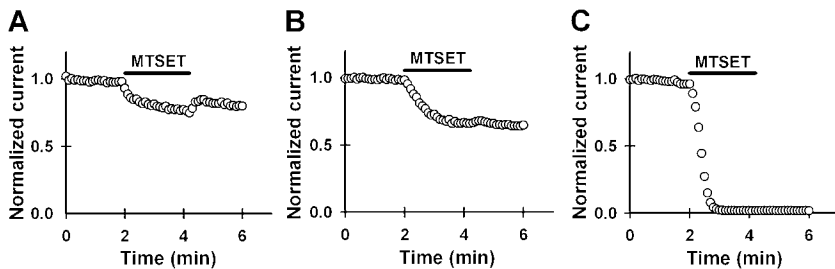

Figure 4. Examples of different effects of MTSET on cysteine mutant channels. (A) Time course of little inhibition of IS6-V3C by internal MTSET. 4 mM MTSET was applied continuously for 2 min. Current was evoked from a holding potential of -80 mV every 6 s by a 500-ms depolarization to a voltage that gives >70% channel open probability. (B and C) Time course of partial inhibition of IIIS6-P13C (B) and complete inhibition of IIS6-V1C (C) by internal MTSET. Experiment conditions were the same as in A.
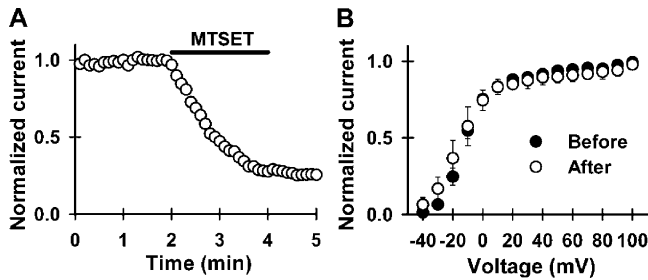
Figure 6. Gating is not changed after modification by MTSET. (A) Time course of inhibition of a representative mutant channel, IS6-L2C, by 4 mM internal MTSET. (B) Voltage dependence of activation of IS-L2C before (filled circle) and after (open circle) MTSET application ($n = 6$).

Figure 8. Effect of qBBr on the control channel and two S6 mutant channels. (A) Time course of inhibition of IIIS6-V9C by 4 mM internal qBBr. (B) Bars represent current inhibition of the control and mutant channels by 4 mM qBBr applied to the intracellular side for 8 min. Steady-state inhibition was not reached due to the slow modification.

accessibility does not fit any known sequence alignment with K^+ channels and suggests the existence of an aqueous pathway for MTSET behind S6. If this were the case, one would expect that some positions on the S5 segments, which are likely to be immediately adjacent to and surround the S6 segments as in K^+ channels, would be accessible to internal MTSET. To test this possibility, we substituted all IIIS5 residues and eight residues at the intracellular end of IIS5 and IVS5 with cysteines and examined their accessibility to internal MTSET. Because there is no reactive position on the back side of IS6 (Fig. 5), we decided not to test IS5.

In IIS5 and IVS5 segments, the first position, which presumably lies at the membrane/cytoplasm interface, was reactive to internal MTSET. More important, position 6 in IIIS5 and positions 3 and 8 in IVS5, which are located deep in the membrane, also showed apparent
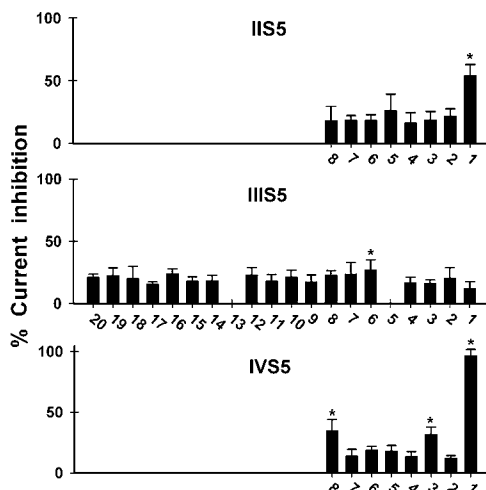

Figure 7. Summary of the effect of MTSET on S5 mutant channels. Bars represent current inhibition by 4 mM internal MTSET on S5 cysteine mutant channels ($n = 3$–8). Stars indicate the mutant channels that were significantly inhibited compared with the control channel ($P < 0.05$). Mutants bearing the cysteine mutation in positions 5 and 13 in IIIS5 failed to produce functional channels.
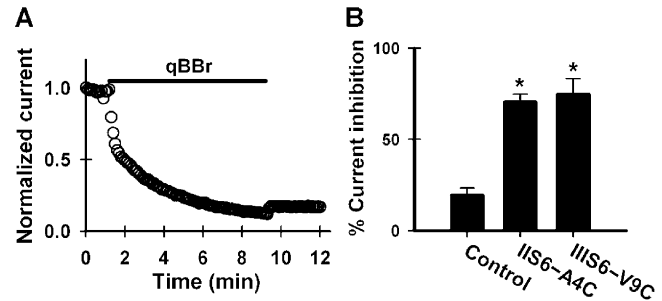
modification (Fig. 7). The current inhibition caused by MTSET was small, but nevertheless, it was significant. Since MTSET is permanently charged and does not partition into the membrane, modification of these S5 positions suggests that either some portions of S5 contribute to form the inner pore or there is an aqueous crevice between S5 and S6. The latter seems more likely since in K^+ channels the S5 segments are clearly behind the pore. If this is indeed the case, the current inhibition caused by MTSET modification is then an allosteric effect rather than a direct block of the pore.

The Inner Pore Can Open to 10 Å

In our experiments, by introducing a single cysteine into an S6 segment, only one MTSET moiety is attached to an accessible cysteine. It was thus surprising that some S6 mutant channels were almost completely inhibited by MTSET (e.g., IIS6-A4C, IIIS6-V9C, Fig. 3). Does this mean that the inner pore at those regions is as narrow as 5.8 Å in diameter, which is the dimension of the MTSET head group? To explore the dimension of the inner pore, we tested modification of selected S6 cysteines by another positively charged sulfhydryl-specific reagent qBBr, which is rigid and has a dimension of 12 Å × 10 Å × 6 Å. qBBr produced a clear and large inhibition of IIS6-A4C and IIIS6-V9C channels (Fig. 8), although the speed of modification was much slower than that by MTSET. Considering the rigidity of qBBr, the inner pore must open to at least 10 Å to accommodate this molecule.

DISCUSSION

Knowledge of the structure of the inner pore is important for understanding the mechanisms of ion permeation, drug binding, and gating. In this study, we investigated the architecture of the inner pore of VGCCs using site-directed chemical modification. Our results reveal that the S6 transmembrane segments form a

TABLE II
Summary of the Effect of MTSET on IIS6 Cysteine Mutant Channels

	Positions in IIS6	MTSET inhibition	Reversal potential	Activation $V_{1/2}$	Slope factor k	τ at 0 mV	Inactivation before modification	Inactivation after modification
		%	mV	mV	mV	ms	%	%
WT		100.0 ± 0.0 (6)	84.4 ± 2.8	26.0 ± 2.6	8.6 ± 1.3	4.4 ± 2.0[a]	9.5 ± 3.9	
Control		19.0 ± 5.9 (20)	82.7 ± 4.8	6.6 ± 3.6	9.0 ± 0.9	5.4 ± 2.2	8.1 ± 4.2	14.5 ± 4.4
G701C	14	11.2 ± 7.2 (5)	76.2 ± 4.8	−17.6 ± 2.8	7.3 ± 0.6	2.8 ± 0.4	2.6 ± 2.3	3.4 ± 2.3
N702C	13	43.0 ± 5.5 (7)	82.0 ± 4.5	−1.1 ± 6.3	8.9 ± 1.5	4.2 ± 0.9	24.4 ± 13.6	25.9 ± 6.8
Y703C	12	41.9 ± 12.4 (9)	82.0 ± 3.4	17.0 ± 3.6	11.7 ± 1.2	3.4 ± 1.2	48.4 ± 15.7	54.6 ± 18.6
T704C	11	28.4 ± 9.2 (11)	82.5 ± 4.1	7.6 ± 3.6	10.1 ± 0.7	5.0 ± 2.1	16.8 ± 10.4	30.4 ± 16.8
L705C	10	85.8 ± 2.6 (4)	75.8 ± 8.3	−6.0 ± 1.6	6.9 ± 0.6	5.6 ± 1.0	28.0 ± 10.4	
L706C	9	55.5 ± 8.3 (5)	83.4 ± 2.4	19.8 ± 2.2	12.8 ± 0.6	2.8 ± 0.6	25.2 ± 8.8	39.2 ± 4.9
N707C	8	56.2 ± 2.4 (4)	83.0 ± 0.8	5.0 ± 3.8	9.0 ± 1.6	6.6 ± 2.9	74.5 ± 10.4	90.5 ± 6.8
V708C	7	16.6 ± 2.8 (4)	67.3 ± 8.4	−12.1 ± 4.4	8.9 ± 0.8	2.4 ± 1.2	3.1 ± 2.5	2.4 ± 4.2
F709C	6	20.1 ± 2.3 (5)	64.2 ± 7.6	−14.3 ± 7.8	7.2 ± 3.5	3.9 ± 2.1	2.3 ± 1.9	2.7 ± 3.2
L710C	5	87.7 ± 2.3 (3)	65.0 ± 7.1	−10.1 ± 4.6	8.7 ± 0.3	4.9 ± 1.2	5.8 ± 3.3	
A711C	4	99.2 ± 1.2 (4)	86.8 ± 2.8	−2.1 ± 4.0	7.0 ± 1.6	6.4 ± 2.5	28.9 ± 10.9	
I712C	3	35.6 ± 3.9 (7)	60.0 ± 19.6	−22.8 ± 9.8	8.8 ± 1.2	2.9 ± 1.4	2.2 ± 1.7	1.2 ± 2.7
A713C	2	78.7 ± 4.1 (4)	77.8 ± 1.3	−5.6 ± 5.0	6.9 ± 1.1	2.6 ± 1.0	7.2 ± 4.7	16.8 ± 3.5
V714C	1	100.0 ± 0.0 (3)	83.3 ± 0.6	1.3 ± 5.1	8.6 ± 0.8	10.3 ± 8.0	11.6 ± 3.2	
D715C	0	77.3 ± 4.8 (4)	74.3 ± 6.1	6.2 ± 3.2	9.8 ± 1.3	5.7 ± 3.8	17.9 ± 5.9	8.8 ± 2.1
N716C	−1	−55.6 ± 16.5 (7)	70.4 ± 3.5	8.6 ± 3.6	11.6 ± 1.8	2.7 ± 0.6	22.3 ± 9.8	15.3 ± 4.6
L717C	−2	9.6 ± 11.5 (5)	82.2 ± 5.4	8.9 ± 3.7	14.4 ± 2.0	2.5 ± 0.4	15.7 ± 5.5	21.2 ± 5.7
A718C	−3	61.2 ± 7.6 (5)	77.8 ± 8.7	−0.9 ± 3.3	9.5 ± 0.2	2.9 ± 0.4	15.9 ± 5.5	20.8 ± 5.0

[a]Same as in Table I.

wide inner pore, which has some unique and unexpected properties.

Pore-lining vs. Nonpore-lining Residues

A key assumption in using SCAM to identify pore-lining residues is that the cysteine mutation by itself does not alter the side-chain orientation of the substituted residue and the overall structure of the channel. This assumption is difficult to verify directly, but the fact that the functional properties of many mutant channels were not significantly altered by the cysteine mutation (Tables I–IV) suggests that it holds true for those channels. However, many other mutant channels (such as L354C, N707C, I712C, N1513C, and I1514C, to give a few examples) did show significant changes in their activation and/or inactivation properties (Tables I–IV). Some of the changes were probably caused by the highly variable contamination from the Cl$^-$ current mediated by the endogenous Ca^{2+}-activated Cl$^-$ channels, which can also be activated to a lesser degree by Ba^{2+}, the charge carrier used in our experiments. Other changes could be genuine since the S6 segments are intimately involved in both activation (Xie et al., 2005) and inactivation gating in VGCCs (for review see Hering et al., 2000; Stotz and Zamponi, 2001). For these mutant channels, we can only hope that the aforementioned assumption also holds true. This hope, however, is not a completely blind one since in K$^+$

channels, where many S6/M2 cysteine mutations also greatly altered various channel properties, the putative pore-lining residues identified by SCAM match nicely those revealed directly by x-ray crystallography (Liu et al., 1997; Doyle et al., 1998; Lu et al., 1999a; Kuo et al., 2003), suggesting that the assumption does hold in K$^+$ channels.

Another key assumption is that when a mutant channel is inhibited by internal MTSET, the corresponding cysteine, and by inference, the original residue, points its side chain to the pore or to an aqueous crevice that is continuous with the pore or the cytoplasm; on the other hand, when a mutant channel is unaffected by internal MTSET, the corresponding residue points its side chain to the membrane or the protein interior. This is a reasonable proposition for S6 residues located within the membrane since MTSET is permanently charged and does not partition into the membrane (Karlin and Akabas, 1998). Although there is a theoretical possibility that modification of a pore-lining residue may be functionally silent, our observation that most of the MTSET-reactive positions form a broad and continuous surface (Fig. 5) makes this possibility seem unlikely.

In this study, accessibility was determined by the change in current amplitude after exposure to MTSET. There are caveats to this approach, particularly for those mutant channels that showed only partial current

TABLE III
Summary of the Effect of MTSET on IIIS6 Cysteine Mutant Channels

	Positions in IIIS6	MTSET inhibition	Reversal potential	Activation $V_{1/2}$	Slope factor k	τ at 0 mV	Inactivation before modification	Inactivation after modification
		%	mV	mV	mV	ms	%	%
WT		100.0 ± 0.0 (6)	84.4 ± 2.8	26.0 ± 2.6	8.6 ± 1.3	4.4 ± 2.0[a]	9.5 ± 3.9	
Control		19.0 ± 5.9 (20)	82.7 ± 4.8	6.6 ± 3.6	9.0 ± 0.9	5.4 ± 2.2	8.1 ± 4.2	14.5 ± 4.4
M1496C	25	18.0 ± 5.9 (10)	82.1 ± 3.2	3.7 ± 3.0	9.9 ± 0.6	3.3 ± 0.9	10.1 ± 4.5	21.3 ± 11.0
I1498C	23	24.4 ± 4.1 (10)	81.2 ± 4.5	8.2 ± 4.0	10.6 ± 0.9	4.6 ± 2.8	14.5 ± 9.2	28.8 ± 13.8
F1499C	22	28.9 ± 7.8 (13)	80.1 ± 5.7	12.6 ± 3.8	11.6 ± 1.5	3.5 ± 0.7	12.9 ± 8.0	25.7 ± 13.9
Y1500C	21	24.6 ± 7.8 (7)	72.0 ± 4.9	3.8 ± 4.7	11.5 ± 1.0	4.0 ± 2.7	11.2 ± 7.5	11.7 ± 4.9
V1502C	19	24.3 ± 7.9 (8)	80.0 ± 5.4	8.2 ± 2.7	10.4 ± 1.5	4.3 ± 1.1	13.9 ± 5.8	28.8 ± 8.8
F1504C	17	13.8 ± 8.1 (4)	82.3 ± 0.5	10.2 ± 2.7	10.5 ± 0.3	8.2 ± 3.8	9.0 ± 1.9	16.6 ± 1.2
V1505C	16	17.3 ± 11.2 (5)	82.1 ± 3.4	12.1 ± 3.9	9.5 ± 0.7	5.2 ± 1.2	11.2 ± 4.0	16.8 ± 4.1
V1506C	15	22.4 ± 4.9 (12)	78.2 ± 6.4	1.6 ± 3.9	10.1 ± 0.9	2.7 ± 0.9	11.2 ± 6.3	23.3 ± 12.9
F1507C	14	22.6 ± 5.9 (5)	82.3 ± 3.1	6.0 ± 1.7	9.9 ± 0.6	4.1 ± 0.4	15.2 ± 7.8	33.8 ± 5.7
P1508C	13	39.0 ± 9.7 (9)	81.9 ± 3.9	7.1 ± 5.3	13.8 ± 2.5	2.9 ± 0.6	19.2 ± 8.2	25.8 ± 11.9
F1509C	12	33.2 ± 11.9 (12)	80.6 ± 6.0	12.8 ± 5.5	11.0 ± 2.8	4.8 ± 2.6	26.7 ± 15.6	40.0 ± 17.8
F1510C	11	27.0 ± 11.9 (15)	79.5 ± 5.1	6.8 ± 4.7	8.6 ± 1.0	5.2 ± 4.9	20.7 ± 12.0	30.2 ± 18.1
F1511C	10	17.7 ± 6.5 (4)	73.3 ± 10.9	−5.7 ± 4.1	8.2 ± 1.6	4.0 ± 2.4	15.7 ± 10.0	24.1 ± 12.6
V1512C	9	93.0 ± 1.6 (4)	73.7 ± 6.1	1.8 ± 4.8	8.0 ± 0.5	5.2 ± 4.3	25.8 ± 6.7	52.2 ± 10.6
N1513C	8	42.0 ± 6.4 (4)	86.0 ± 1.6	1.7 ± 1.9	8.7 ± 1.8	4.3 ± 0.7	86.0 ± 7.4	96.1 ± 4.5
I1514C	7	39.8 ± 6.1 (5)	75.6 ± 18.0	41.1 ± 13.1	15.9 ± 1.0	1.7 ± 0.2	19.9 ± 8.9	25.0 ± 12.3
F1515C	6	13.1 ± 2.7 (5)	80.2 ± 5.1	−6.0 ± 4.2	9.2 ± 0.9	2.9 ± 1.1	11.2 ± 3.6	12.9 ± 3.8
V1516C	5	43.6 ± 9.2 (4)	69.5 ± 19.1	8.5 ± 5.4	10.4 ± 1.6	5.4 ± 0.1	5.8 ± 4.0	7.9 ± 6.9
A1517C	4	73.6 ± 10.0 (5)	75.6 ± 10.3	−9.8 ± 7.1	6.8 ± 0.7	6.0 ± 1.9	16.0 ± 3.5	15.7 ± 10.6
L1518C	3	24.0 ± 3.6 (6)	82.7 ± 3.4	18.9 ± 7.3	16.2 ± 4.4	2.1 ± 0.6	30.3 ± 17.9	27.4 ± 16.2
I1519C	2	35.1 ± 10.8 (8)	81.6 ± 5.1	−2.4 ± 5.4	7.6 ± 1.2	5.7 ± 2.2	20.0 ± 8.4	38.4 ± 16.8
I1520C	1	52.6 ± 4.1 (4)	60.0 ± 13.1	−7.5 ± 3.7	6.9 ± 1.1	3.9 ± 2.0	7.8 ± 9.3	11.3 ± 15.7
I1521C	0	30.3 ± 4.0 (4)	74.0 ± 2.2	10.0 ± 1.9	11.1 ± 0.5	6.8 ± 2.3	54.3 ± 13.1	16.2 ± 10.1
T1522C	−1	45.3 ± 7.0 (7)	72.9 ± 3.7	−9.0 ± 7.1	12.3 ± 1.9	2.3 ± 0.6	35.8 ± 7.6	14.3 ± 7.2
F1523C	−2	35.5 ± 7.4 (4)	75.5 ± 3.9	−6.2 ± 3.1	9.3 ± 1.0	1.9 ± 0.5	13.9 ± 3.3	23.3 ± 4.5
Q1524C	−3	42.4 ± 4.0 (4)	85.8 ± 2.5	9.0 ± 4.8	7.8 ± 1.0	5.2 ± 1.9	10.2 ± 3.7	17.4 ± 4.6

[a]Same as in Table I.

inhibition (Fig. 3). The partial inhibition itself is not surprising, since only a single cysteine in one of the four pore-lining segments was modified. In K⁺ channels, modification of a single cysteine in one of the four subunits also produces only 10–25% inhibition (Lu et al., 1999a; Loussouarn et al., 2001). The partial inhibition we observed in this study could not be attributed to channel rundown since we could clearly and easily separate the two processes (e.g., Fig. 4 B). But could it be a nonspecific effect, at least for those mutant channels where an extended period of time (up to 4 min) of MTSET exposure was required to achieve steady-state inhibition? We cannot exclude this possibility, but two reasons argue against it. First, in each S6 segment, most of the reactive positions form a continuous face, bordered by positions 4 and 13 (Fig. 5), rather than dot randomly, as would be expected if modification occurred at random as a result of spontaneous dynamic conformational changes of the channel protein. Second, in our previous work on Kir2.1 channels, we also

observed several positions that were modified partially and slowly (Lu et al., 1999a). Those positions correspond to pore-lining positions in the KcsA and MthK crystal structure (Doyle et al., 1998; Jiang et al., 2002b).

Ca²⁺ Channel Inner Pore Is Asymmetric

The inner pore of K⁺ channels is formed by the S6/M2 segments from four identical subunits. The inner pore of VGCCs, on the other hand, is formed by the S6 segments from four homologous but nonidentical repeats. Thus, there is an intrinsic amino acid sequence asymmetry to the Ca²⁺ pore. This asymmetry is also demonstrated by the differential functional impact of MTSET modification. For instance, position 10 was modified in both IIS6 and IVS6, but the resulting current inhibition was dramatically different (85.8 ± 2.6% vs. 31.4 ± 8.8%); furthermore, the same position was not modified in IS6 and IIIS6 (Fig. 3). Another example is that positions 1 and 2 were modified in every repeat; however, the current inhibition was ~100% and >70% in

TABLE IV
Summary of the Effect of MTSET on IVS6 Cysteine Mutant Channels

	Positions in IVS6	MTSET inhibition	Reversal potential	Activation $V_{1/2}$	Slope factor k	τ at 0 mV	Inactivation before modification	Inactivation after modification
		%	mV	mV	mV	ms	%	%
WT		100.0 ± 0.0 (6)	84.4 ± 2.8	26.0 ± 2.6	8.6 ± 1.3	4.4 ± 2.0[a]	9.5 ± 3.9	
Control		19.0 ± 5.9 (20)	82.7 ± 4.8	6.6 ± 3.6	9.0 ± 0.9	5.4 ± 2.2	8.1 ± 4.2	14.5 ± 4.4
S1802C	19	33.8 ± 3.1 (5)	82.0 ± 4.6	5.5 ± 3.2	9.3 ± 0.6	3.4 ± 0.6	12.1 ± 3.0	27.9 ± 3.3
F1803C	18	27.3 ± 9.8 (9)	78.0 ± 6.7	11.2 ± 5.5	9.3 ± 1.0	7.7 ± 4.0	20.8 ± 7.3	35.1 ± 12.2
I1804C	17	22.2 ± 2.6 (4)	77.8 ± 4.3	6.9 ± 4.8	10.5 ± 0.7	3.9 ± 0.3	13.5 ± 5.9	19.9 ± 7.0
F1805C	16	27.7 ± 13.9 (12)	83.5 ± 4.5	3.6 ± 2.4	8.7 ± 0.8	6.3 ± 3.6	18.6 ± 8.8	39.7 ± 13.1
L1806C	15	21.1 ± 6.8 (11)	81.9 ± 3.0	7.4 ± 4.2	9.7 ± 1.2	3.3 ± 1.2	16.3 ± 6.9	26.7 ± 12.4
C1807C	14	26.5 ± 14.4 (7)	78.4 ± 7.9	13.6 ± 2.9	11.8 ± 2.0	4.2 ± 1.7	25.5 ± 15.1	37.6 ± 16.1
S1808C	13	65.5 ± 9.0 (7)	78.1 ± 3.9	14.8 ± 4.5	12.6 ± 1.2	5.3 ± 3.1	15.0 ± 5.9	31.6 ± 12.5
F1809C	12	44.1 ± 8.5 (9)	77.0 ± 6.3	3.4 ± 2.6	9.9 ± 0.8	4.9 ± 2.8	13.6 ± 6.9	17.3 ± 10.4
L1810C	11	20.5 ± 1.8 (3)	69.3 ± 3.1	4.2 ± 3.5	10.6 ± 1.1	2.6 ± 0.5	14.3 ± 3.5	25.7 ± 2.5
M1811C	10	31.4 ± 8.8 (8)	84.0 ± 2.7	21.4 ± 4.8	13.5 ± 2.0	3.2 ± 0.7	21.8 ± 10.5	34.6 ± 8.3
L1812C	9	56.5 ± 12.7 (5)	80.4 ± 5.1	14.5 ± 4.2	14.0 ± 3.8	4.2 ± 1.5	34.4 ± 13.9	54.2 ± 11.1
F1815C	6	21.5 ± 9.7 (11)	78.5 ± 6.7	10.4 ± 4.1	11.6 ± 1.6	4.1 ± 1.8	17.2 ± 11.1	34.7 ± 23.5
V1816C	5	59.4 ± 5.4 (5)	82.0 ± 2.8	4.6 ± 2.4	9.3 ± 0.8	4.7 ± 2.3	28.6 ± 9.1	50.5 ± 11.0
A1817C	4	100.0 ± 0.0 (4)	79.0 ± 8.5	8.1 ± 3.1	10.3 ± 1.0	4.3 ± 1.2	33.9 ± 9.3	
V1818C	3	25.0 ± 6.6 (9)	80.2 ± 4.7	−6.7 ± 4.7	7.9 ± 1.0	5.3 ± 3.0	6.4 ± 3.1	6.6 ± 4.8
I1819C	2	93.2 ± 6.4 (6)	77.0 ± 3.5	7.9 ± 3.4	11.2 ± 1.1	6.1 ± 3.9	17.2 ± 3.9	
M1820C	1	99.7 ± 0.6 (5)	78.2 ± 3.5	8.7 ± 4.6	9.0 ± 0.9	2.9 ± 0.9	54.1 ± 16.3	
D1821C	0	77.4 ± 4.0 (6)	81.5 ± 3.7	4.9 ± 2.9	7.2 ± 0.5	4.3 ± 1.2	26.2 ± 3.3	50.8 ± 15.7
N1822C	−1	58.0 ± 3.7 (4)	86.3 ± 3.5	10.8 ± 2.0	11.2 ± 0.2	3.5 ± 0.4	26.7 ± 7.9	23.9 ± 20.2
F1823C	−2	54.1 ± 9.2 (5)	76.0 ± 4.5	6.9 ± 4.2	8.3 ± 0.8	3.9 ± 1.5	22.8 ± 16.5	24.4 ± 12.0
E1824C	−3	53.3 ± 7.8 (5)	77.0 ± 7.4	11.8 ± 6.9	8.2 ± 0.7	7.6 ± 2.5	18.5 ± 7.6	16.2 ± 8.3

[a]Same as in Table I.

IS6, IIS6, and IVS6, but only 52.6 ± 4.1% and 35.1 ± 10.8% in IIIS6 (Fig. 3). These results lend support to the notion that the four S6 segments of VGCCs are functionally nonequivalent, as has been demonstrated by their differential role in the binding of DHPs, PAAs, and BTZs (see below for more discussion). They also suggest that the vertical position and/or orientation of the four S6 segments may be different.

S6 and S5 Transmembrane Segments May Be Loosely Packed

Based on various amino acid sequence alignments, several homology models of the inner pore of VGCCs have been proposed using the crystal structure of KcsA K^{+} channel as a template (Huber et al., 2000; Zhorov et al., 2001; Lipkind and Fozzard, 2003). The modification pattern of the S6 segments of VGCCs obtained in this study does not fit any of the current homology models and is strikingly different from that of K^{+} channels (Liu et al., 1997; Lu et al., 1999a). One major difference is that many more positions above the putative membrane/cytoplasm interface are reactive to MTSET in Ca^{2+} channels than in K^{+} channels (Fig. 5). Another major difference is that in IIS6, IIIS6, and IVS6 of Ca^{2+} channels, one or two positions on the opposite or back side of the accessible surface, which most likely forms the lining of the inner pore, are also modified by internal MTSET. This observation suggests that either these S6 segments are not a continuous α-helix, which seems unlikely based on secondary structure predictions and the structure of the K^{+} channel S6/M2 segments, or the pore-lining S6 and surrounding S5 segments are loosely packed, creating an aqueous crevice in between. Consistent with the latter hypothesis, several positions in the S5 segments, some of which are buried deep in the membrane, were found to react with internal MTSET (Fig. 7). The current inhibition caused by modification of these positions is most likely an allosteric effect instead of a direct pore block. It is possible that some other S5 positions were also modified, but their modification was functionally mute.

This type of loose packing between the S5 and S6 transmembrane segments is not present in K^{+} channels. Our previous study on Kir2.1 channels found that none of the M1 positions were modified by either MTSET or MTSEA, even after long exposure to high concentrations of the modifying reagents (Lu et al., 1999a). More important, the crystal structures of KcsA, MthK, and K$_v$AP all show that M1/S5 is buried in membrane lipids and is positioned immediately behind the
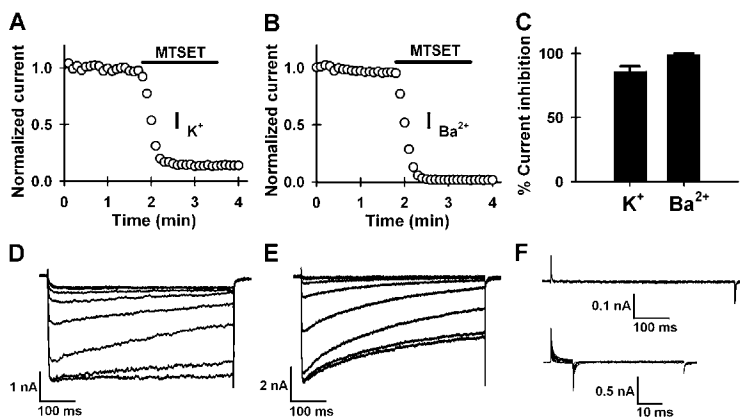
Figure 9. Inhibition of divalent and monovalent current by MTSET. (A and B) Time course of inhibition of monovalent (K^+) current (A) and divalent (Ba^{2+}) current (B) of IIS6-A4C by internal MTSET. (C) Bar graph summarizing the degree of inhibition of monovalent and divalent current. (D and E) Exemplar monovalent (D) and divalent current traces (E) during MTSET inhibition. Monovalent current was evoked from a holding potential of -100 mV every 6 s by a 500-ms depolarization to -30 mV. Divalent current was evoked by the same voltage protocol as in Fig. 1 B. (F) Absence of endogenous monovalent current from uninjected oocytes at -30 mV (top traces) and all voltages from -80 to $+60$ mV (bottom traces, currents were evoked from a holding potential of -100 mV every 3 s by 10-ms depolarizations from -80 to $+60$ mV in 10-mV increments, followed by a 50-ms repolarization to -80 mV).

pore-forming M2/S6 (Doyle et al., 1998; Jiang et al., 2002a, 2003a). There is clearly no aqueous crevice between M1/S5 and M2/S6 that could accommodate a molecule as big as MTSET.

Ca^{2+} Channel Inner Pore Is Wide

Our results show that many S6 mutant channels were inhibited by MTSET by varying degrees (Fig. 3). It is possible that for channels that are inhibited partially, the side chain of the modified positions points tangentially to the pore, whereas for those that are inhibited by a relatively large degree ($>80\%$), their side chain points to the pore more or less perpendicularly. Interestingly, several mutant channels are almost completely inhibited, despite the fact that each mutant channel contains only a single modifiable cysteine in a particular repeat. This is strikingly different from what has been observed in K^+ channels, where modification of cysteines on all four subunits is required to produce complete inhibition (Lu et al., 1999a; Loussouarn et al., 2001).

To explain this discrepancy between Ca^{2+} and K^+ channels, we first need to understand how MTSET modification impedes ion conduction in Ca^{2+} channels. Is it by electrostatic repulsion or physical obstruction, or both? To address this question, we examined the effect of MTSEA on IIIS6-V9C, which was almost completely inhibited by MTSET. MTSEA also carries a single positive charge but has a smaller head group ($\sim$3.6 Å in diameter) than MTSET does. However, it inhibited the current by a similar degree as MTSET did (87.3% and 93.0%, respectively; MTSEA inhibited the control channel by 16.8%) and the modification was faster (unpublished data). This result suggests that electrostatic repulsion between the head group of a modifying reagent and the permeant ions plays a predominant role in blocking the current flow. The much stronger inhibition by MTSET in Ca^{2+} channels is because the charge carrier is a divalent cation (Ba^{2+}), which naturally leads to stronger electrostatic repulsion. Another piece of evidence supporting this interpretation is the weaker effect of MTSET modification on monovalent currents in Ca^{2+} channels. To record a monovalent current, we used the same solution on both sides of the membrane patch, with K^+ as the charge carrier. The K^+ current of IIS6-A4C was inhibited by 86.3% ($n = 6$), whereas the Ba^{2+} current was inhibited by 99.2% ($n = 4$) (Fig. 9). The residual K^+ current ($\sim$14%) was not mediated by endogenous K^+ channels, since it was substantially larger than the endogenous K^+ currents recorded from oocytes lacking exogenously expressed Ca^{2+} channels (Fig. 9, compare D and F).

Chemical modification and x-ray crystallography indicate that the inner pore of K^+ channels can open to $\sim$12 Å (Lu et al., 1999a; Jiang et al., 2002b). Previous work on VGCCs suggests that they may also have a large inner pore. For example, tetramethylammonium, which has a diameter of $\sim$6 Å, can pass through the channel (McCleskey and Almers, 1985). Large organic molecules such as PAAs, BTZs, and DHPs are thought to bind within or close to the ion conduction pathway (Hockerman et al., 1997b). Our finding that qBBr can modify residues deep in the inner pore (Fig. 8) suggests that the Ca^{2+} channel inner pore can open to $>$10 Å.

Implications for the Binding of DHPs and PAAs

Our results have important implications for understanding the mechanism of the binding and actions of

Figure 10. Amino acid sequence alignment of IIIS6 and IVS6 of $Ca_v2.1$ with those of $Ca_v1.2$. The bold and underlined residues in IIIS6 and IVS6 of $Ca_v1.2$ represent residues whose mutations affect the binding of DHPs and PAAs, respectively. Stars indicate MTSET-reactive residues in $Ca_v2.1$.

DHPs, PAAs, and BTZs, drugs that are widely used for the treatment of cardiovascular diseases. DHPs act on L-type Ca^{2+} channel as either agonists favoring the open state or antagonists favoring the inactivated state. Peptide segments contributing to form the DHP-binding site have been localized to IIIS6 and IVS6 of the α_1 subunit by photoaffinity labeling and antibody mapping (Nakayama et al., 1991; Striessnig et al., 1991; Kalasz et al., 1993). Site-directed mutagenesis studies have identified single amino acid residues in IIIS6 and IVS6 whose mutations affected DHP binding (Peterson et al., 1996, 1997). These residues are believed to form a high-affinity DHP-binding site. If we align the amino acid sequence of P/Q-type channels with that of L-type channels (Fig. 10), 5 out of the 10 homologous DHP-binding residues were not modified by MTSET (IIIS6: F11C, F14C, and F17C; IVS6: F16C and I17C). Only three of them showed modification (IIIS6-V9C; IVS6: L9C and M10C). The other two cysteine mutant channels (IIIS6-Y18C and IVS6-N8C) did not produce enough Ba^{2+} current. DHPs are lipophilic compounds that reach their receptor site through the membrane and they are thought to be allosteric modulators (Peterson et al., 1996, 1997; Hockerman et al., 1997b). Our finding that many of the putative DHP-binding residues point away from the pore is in agreement with the idea that DHPs affect channel activity allosterically rather than by blocking the pore directly.

PAAs are another class of high-affinity L-type channel blockers. A number of amino acid residues in IIIS6 and IVS6 have been shown to be important for PAA binding (Hockerman et al., 1995, 1997a,b), some of which are also involved in DHP binding. It has been hypothesized that PAAs and DHPs bind to different faces of IIIS6 and IVS6 and in some cases to opposite sides of the same amino acid residues (Hockerman et al., 1997b). While DHPs affect channel activity allosterically, PAAs block the pore directly (Hockerman et al., 1995, 1997a,b). However, among the seven analogous putative PAA-binding residues in P/Q-type channels, only three (IIIS6-V5C; IVS6: M10C and S13C) were modified by MTSET (Fig. 10). Except for IIIS6-Y18C that did not produce enough Ba^{2+} current, the other three residues were not modified and are therefore unlikely to line the pore. These results suggest that some of the residues whose mutations affect PAA block may not participate directly in PAA binding or part of PAA may interact with hydrophobic residues pointing away from the pore.

Several models have been proposed for the binding of DHPs and PAAs to Ca^{2+} channels (Huber et al., 2000; Zhorov et al., 2001; Lipkind and Fozzard, 2003). They are all based on the KcsA structure and therefore need further improvement. Our results provide data for constructing a more realistic model. In particular, the proposed loose packing between the S5 and S6 transmembrane segments in VGCCs should be a key consideration in future modeling. This loose packing may confer certain flexibility to the S5 and S6 segments that would permit the creation of a binding pocket suitable for bulky molecules such as DHPs, PAAs, and BTZs.

REFERENCES

Akabas, M.H., D.A. Stauffer, M. Xu, and A. Karlin. 1992. Acetylcholine-receptor channel structure probed in cysteine-substitution mutants. *Science.* 258:307–310.

Akabas, M.H., C. Kaufmann, P. Archdeacon, and A. Karlin. 1994. Identification of acetylcholine-receptor channel-lining residues in the entire M2 segment of the α-subunit. *Neuron.* 13:919–927.

Catterall, W.A. 2000. Structure and regulation of voltage-gated Ca^{2+} channels. *Annu. Rev. Cell Dev. Biol.* 16:521–555.

del Camino, D., and G. Yellen. 2001. Tight steric closure at the intracellular activation gate of a voltage-gated K^+ channel. *Neuron.* 32:649–656.

Doyle, D.A., J.M. Cabral, R.A. Pfuetzner, A.L. Kuo, J.M. Gulbis, S.L. Cohen, B.T. Chait, and R. MacKinnon. 1998. The structure of the potassium channel: molecular basis of K^+ conduction and selectivity. *Science.* 280:69–77.

Ellinor, P.T., J. Yang, W.A. Sather, J.F. Zhang, and R.W. Tsien. 1995. Ca^{2+} channel selectivity at a single-locus for high-affinity Ca^{2+} interactions. *Neuron.* 15:1121–1132.

Flynn, G.E., and W.N. Zagotta. 2001. Conformational changes in S6 coupled to the opening of cyclic nucleotide-gated channels. *Neuron.* 30:689–698.

Hering, S., S. Berjukow, S. Sokolov, R. Marksteiner, R.G. Weiss, R. Kraus, and E.N. Timin. 2000. Molecular determinants of inactivation in voltage-gated Ca^{2+} channels. *J. Physiol.* 528:237–249.

Hockerman, G.H., B.D. Johnson, T. Scheuer, and W.A. Catterall. 1995. Molecular determinants of high-affinity phenylalkylamine block of L-type calcium channels. *J. Biol. Chem.* 270:22119–22122.

Hockerman, G.H., B.D. Johnson, M.R. Abbott, T. Scheuer, and W.A. Catterall. 1997a. Molecular determinants of high affinity phenylalkylamine block of L-type calcium channels in transmembrane segment IIIS6 and the pore region of the α1 subunit. *J. Biol. Chem.* 272:18759–18765.

Hockerman, G.H., B.Z. Peterson, B.D. Johnson, and W.A. Catterall. 1997b. Molecular determinants of drug binding and action on L-type calcium channels. *Annu. Rev. Pharmacol. Toxicol.* 37:361–396.

Huber, I., E. Wappl, A. Herzog, J. Mitterdorfer, H. Glossmann, T. Langer, and J. Striessnig. 2000. Conserved Ca^{2+}-antagonist-binding properties and putative folding structure of a recombinant high-affinity dihydropyridine-binding domain. *Biochem. J.* 347:829–836.

Jiang, Y., A. Lee, J.Y. Chen, M. Cadene, B.T. Chait, and R. MacKinnon. 2002a. Crystal structure and mechanism of a calcium-gated potassium channel. *Nature.* 417:515–522.

Jiang, Y., A. Lee, J.Y. Chen, M. Cadene, B.T. Chait, and R. MacKin-

non. 2002b. The open pore conformation of potassium channels. *Nature.* 417:523–526.

Jiang, Y., A. Lee, J.Y. Chen, V. Ruta, M. Cadene, B.T. Chait, and R. MacKinnon. 2003a. X-ray structure of a voltage-dependent K^+ channel. *Nature.* 423:33–41.

Jiang, Y., V. Ruta, J.Y. Chen, A. Lee, and R. MacKinnon. 2003b. The principle of gating charge movement in a voltage-dependent K^+ channel. *Nature.* 423:42–48.

Kalasz, H., T. Watanabe, H. Yabana, K. Itagaki, K. Naito, H. Nakayama, A. Schwartz, and P.L. Vaghy. 1993. Identification of 1,4-dihydropyridine binding domains within the primary structure of the α-1 subunit of the skeletal-muscle L-type calcium-channel. *FEBS Lett.* 331:177–181.

Karlin, A., and M.H. Akabas. 1998. Substituted-cysteine accessibility method. *Methods Enzymol.* 293:123–145.

Kim, M.S., T. Morii, L.X. Sun, K. Imoto, and Y. Mori. 1993. Structural determinants of ion selectivity in brain calcium-channel. *FEBS Lett.* 318:145–148.

Kuo, A., J.M. Gulbis, J.F. Antcliff, T. Rahman, E.D. Lowe, J. Zimmer, J. Cuthbertson, F.M. Ashcroft, T. Ezaki, and D.A. Doyle. 2003. Crystal structure of the potassium channel KirBac1.1 in the closed state. *Science.* 300:1922–1926.

Lipkind, G.M., and H.A. Fozzard. 2003. Molecular modeling of interactions of dihydropyridines and phenylalkylamines with the inner pore of the L-type Ca^{2+} channel. *Mol. Pharmacol.* 63:499–511.

Liu, J., and S.A. Siegelbaum. 2000. Change of pore helix conformational state upon opening of cyclic nucleotide-gated channels. *Neuron.* 28:899–909.

Liu, Y., M. Holmgren, M.E. Jurman, and G. Yellen. 1997. Gated access to the pore of a voltage-dependent K^+ channel. *Neuron.* 19: 175–184.

Loussouarn, G., L.R. Phillips, R. Masia, T. Rose, and C.G. Nichols. 2001. Flexibility of the Kir6.2 inward rectifier K^+ channel pore. *Proc. Natl. Acad. Sci. USA.* 98:4227–4232.

Lu, T., B. Nguyen, X.M. Zhang, and J. Yang. 1999a. Architecture of a K^+ channel inner pore revealed by stoichiometric covalent modification. *Neuron.* 22:571–580.

Lu, T., Y.G. Zhu, and J. Yang. 1999b. Cytoplasmic amino and carboxyl domains form a wide intracellular vestibule in an inwardly rectifying potassium channel. *Proc. Natl. Acad. Sci. USA.* 96:9926–9931.

McCleskey, E.W., and W. Almers. 1985. The Ca channel in skeletal-muscle is a large pore. *Proc. Natl. Acad. Sci. USA.* 82:7149–7153.

Mikami, A., K. Imoto, T. Tanabe, T. Niidome, Y. Mori, H. Takeshima, S. Narumiya, and S. Numa. 1989. Primary structure and functional expression of the cardiac dihydropyridine-sensitive calcium channel. *Nature.* 340:230–233.

Nakayama, H., M. Taki, J. Striessnig, H. Glossmann, W.A. Catterall, and Y. Kanaoka. 1991. Identification of 1,4-dihydropyridine binding regions within the α-1 subunit of skeletal-muscle Ca^{2+} channels by photoaffinity-labeling with diazipine. *Proc. Natl. Acad. Sci. USA.* 88:9203–9207.

Peterson, B.Z., T.N. Tanada, and W.A. Catterall. 1996. Molecular determinants of high affinity dihydropyridine binding in L-type calcium channels. *J. Biol. Chem.* 271:5293–5296.

Peterson, B.Z., B.D. Johnson, G.H. Hockerman, M. Acheson, T. Scheuer, and W.A. Catterall. 1997. Analysis of the dihydropyridine receptor site of L-type calcium channels by alanine-scanning mutagenesis. *J. Biol. Chem.* 272:18752–18758.

Stotz, S.C., and G.W. Zamponi. 2001. Structural determinants of fast inactivation of high voltage-activated Ca^{2+} channels. *Trends Neurosci.* 24:176–181.

Striessnig, J., B.J. Murphy, and W.A. Catterall. 1991. Dihydropyridine receptor of L-type Ca^{2+} channels - identification of binding domains for $H-3^+$-Pn200-110 and H-3 azidopine within the α-1 subunit. *Proc. Natl. Acad. Sci. USA.* 88:10769–10773.

Tang, S., G. Mikala, A. Bahinski, A. Yatani, G. Varadi, and A. Schwartz. 1993. Molecular localization of ion selectivity sites within the pore of a human L-type cardiac calcium-channel. *J. Biol. Chem.* 268:13026–13029.

Wu, L., C.S. Bauer, X.G. Zhen, C. Xie, and J. Yang. 2002. Dual regulation of voltage-gated calcium channels by PtdIns(4,5)P-2. *Nature.* 419:947–952.

Wu, X.S., H.D. Edwards, and W.A. Sather. 2000. Side chain orientation in the selectivity filter of a voltage- gated Ca^{2+} channel. *J. Biol. Chem.* 275:31778–31785.

Xie, C., X.G. Zhen, and J. Yang. 2005. Localization of the activation gate of a voltage-gated Ca^{2+} channel. *J. Gen. Physiol.* 126:205–212.

Xiao, J., X.G. Zhen, and J. Yang. 2003. Localization of PIP_2 activation gate in inward rectifier K^+ channels. *Nat. Neurosci.* 6:811–818.

Yang, J., P.T. Ellinor, W.A. Sather, J.F. Zhang, and R.W. Tsien. 1993. Molecular determinants of Ca^{2+} selectivity and ion permeation in L-type Ca^{2+} channels. *Nature.* 366:158–161.

Yang, N., and R. Horn. 1995. Evidence for voltage-dependent S4 movement in sodium-channels. *Neuron.* 15:213–218.

Zhorov, B.S., E.V. Folkman, and V.S. Ananthanarayanan. 2001. Homology model of dihydropyridine receptor: implications for L-type Ca^{2+} channel modulation by agonists and antagonists. *Arch. Biochem. Biophys.* 393:22–41.